THE COLDEST PLACES IN HAWAII

The Ice-Preserving Microclimates of High-Altitude Craters and Caves on Tropical Island Volcanoes

Norbert Schörghofer, Steven Businger, and Matthias Leopold

Permafrost and perennial cave ice are preserved in Hawaii as a result of microclimates.

The upper slopes of Hawaii's tallest volcanoes, Mauna Kea and Mauna Loa, are stone deserts where annual-mean temperatures are well above freezing, yet perennial ice is found in a few craters and caves. These ice bodies persist in an exceptionally warm climate. On the summit of Mauna Kea, the mean annual air temperature (MAAT) is +4°C (http://climate.geography.hawaii.edu/). The freezing index (the time integral of all temperature deviations below 0°C) is only about 200°C days yr^{-1}, partly because of the small diurnal and seasonal temperature

AFFILIATIONS: Schörghofer—Institute for Astronomy, University of Hawai'i at Mānoa, Honolulu, Hawaii, and Planetary Science Institute, Tucson, Arizona; Businger—Department of Atmospheric Sciences, University of Hawai'i at Mānoa, Honolulu, Hawaii; Leopold—School of Agriculture and Environment, University of Western Australia, Crawley, Western Australia, Australia
CORRESPONDING AUTHOR: Norbert Schörghofer, norbert@hawaii.edu

amplitudes characteristic of a tropical island. Harris (1981) compiled air freezing indices for sporadic permafrost and ice caves worldwide. The permafrost on Mauna Kea and the ice caves of Mauna Loa are both record holders in terms of freezing indices (see also Niu et al. 2016), which raises the question, What physical phenomena are responsible for these exceptional occurrences of perennial ice?

Craters. Two high-altitude craters on Mauna Kea, Pu'uwēkiu and Pu'uhaukea (Figs. 1 and 2), harbor sporadic permafrost beneath their north-facing *interior* slopes (Woodcock et al. 1970; Schörghofer et al. 2017). If elevation, northerly exposure, and terrain shadowing were the only factors, permafrost would also be expected on steep exterior north-facing slopes. Woodcock (1974) recognized that trapped radiatively cooled air is a microclimatological factor inside Pu'uwēkiu. A third study site is Pu'umākanaka, the deepest cinder cone on Mauna Kea, situated at a lower elevation (Table 1).

Cold-air pools (CAPs), the accumulation of cold air in a closed basin, are a well-known microclimatological phenomenon (e.g., Neff and King 1989; Whiteman et al. 2004; Geiger et al. 2009). Classical examples of sinkholes, such as the Grünloch in Austria and Peter Sinks in Utah, are known for their record low temperatures (e.g., Sauberer and Dirmhirn 1954; Clements et al.
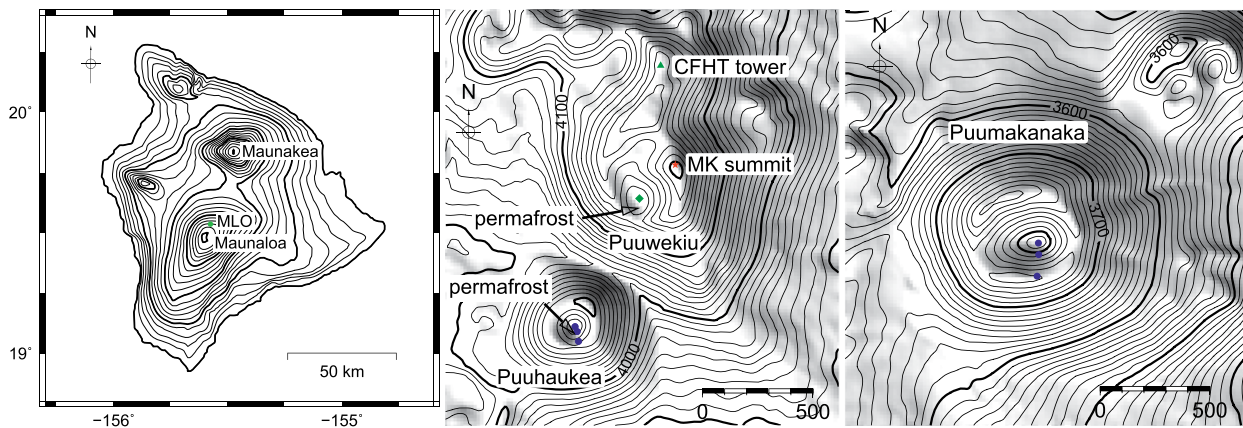
FIG. 1. Topographic maps of the island of Hawaii (250-m contour spacing) and of three cinder cones on Mauna Kea (10-m contour spacing), where our cold-air pool studies were carried out. The green dots indicate meteorological stations, and the red dot marks the summit of Mauna Kea. The three blue dots in Puʻuhaukea and Puʻumākanaka indicate air temperature dataloggers.

2003). Diurnal CAPs are generally dominated by radiative cooling. The strength of the pool (the temperature difference between top and bottom of the pool) can depend on a variety of factors, such as the depth of the basin, the sky view factor, the area of the drainage basin, ground thermal properties, and atmospheric emissivity (e.g., Whiteman et al. 2004). The summit plateau of Mauna Kea is exceptionally dry, and, unlike the aforementioned classical examples, its basins are free of vegetation and rarely covered by snow. Hence, they can serve as an idealized end-member model for microclimate studies, except perhaps for the permeability of the cinder cones (Woodcock and Friedman 1979; Woodcock 1987). Among the few previous studies of the microclimates of craters are Whiteman et al. (2008, 2010), who studied the much larger and lower-lying Meteor Crater in Arizona.

Caves. The other locations on the Hawaiian Islands where perennial ice has been documented are two lava tube caves: Mauna Loa Icecave (MLIC) and Arsia Cave (Pflitsch et al. 2016; Teehera et al. 2018). Unlike Mauna Kea, Mauna Loa is an active volcano with numerous lava tubes (Halliday 2004). The study sites are on the north slope of the giant shield volcano, roughly at the elevation of the Mauna Loa Observatory (MLO; 3,397 m). The MAAT at MLO is +8°C, so a significant cooling mechanism is necessary to allow freezing conditions to prevail throughout the year. From 2011 to 2015, MLO air temperature was below freezing only 0.7% of the time and the freezing index was a mere 2°C days yr^{-1}, practically indistinguishable from zero. In other words, perennial ice is found beneath an environment that rarely ever experiences freezing temperatures.

In his classic work, Balch (1900, p. 148) concluded that "the cold of winter is the source of the cold which produces the ice" (winter's cold theory), in part because cave ice is usually found already near the cave entrance. He argued that cold winter air sinks into a cave, and the removal of sensible heat causes water to freeze, which will then stay frozen because warm air penetrates only with difficulty into the cave. Evaporative cooling can also contribute to freezing conditions (Persoiu and Onac 2011). The latent heat of sublimation is the latent heat of melting plus that of vaporization, and vaporization takes more than 7 times the energy of melting, so removal of vapor is an energetically efficient form of cooling.

TABLE 1. Geometric data for the crater microclimate study sites. The sky view factor is the proportion of sky visible above a viewing point and ranges from 0 to 1. Height, view factor, and drainage area are all relative to the lowest point within the crater.

Cinder cone	Elevation of lowest point on crater floor (m)	Lowest height of crater rim (m)	Sky view factor	Drainage area (km²)	No. of air temperature sensors (averaging interval)
Puʻuwēkiu	4,128	15	0.72	0.119	1 (30 min)
Puʻuhaukea	4,058	34	0.61	0.034	3 (5–30 min)
Puʻumākanaka	3,682	56	0.64	0.152	3 (15 min)

Arsia Cave has two branches (called A and B) with large ice bodies that were continuously frozen from when the cave was discovered in 2009 (and possibly centuries before that) until the summer of 2014 (Fig. 3). Water from surface snowmelt or rain occasionally drips from the cave ceiling, and the clear ice contains centimeter-sized bubbles, which indicates slow freezing from above (Bari and Hallett 1974; Carte 1961). Figure 3 includes a schematic illustration of the cave geometry. Another lava tube, Mauna Loa Icecave, has a much smaller exposed area of perennial ice (Pflitsch et al. 2016). The tubes are ~100–300 m long from the entrance pit to the terminal ice body and, for the most part, tall enough so that a person can walk upright. All three lava tubes gradually slope downhill from the entrance to the ice body, so cold air can sink without obstruction. The only exception is a large pile of breakdown material in branch B of Arsia Cave, which air can still move around laterally.

Here we explore the microclimates in the craters and caves and assess their role for the preservation of perennial ice bodies.

FIG. 2. The interiors of the cinder cones Pu'uwēkiu (Summit Cone Crater), Pu'uhaukea (Goodrich Cone), and Pu'umākanaka. The summit of Mauna Kea lies on the rim of Pu'uwēkiu, and the coldest temperature ever measured in Hawaii has been recorded on the crater floor, where a temporary weather station was installed. Pu'uwēkiu Crater has a diameter of about 300 m. Pu'uhaukea Crater is about 200 m in diameter, and the locations of its three air temperature sensors are labeled L1, L2, and L3. Pu'umākanaka is the deepest cinder cone on Mauna Kea and is about 400 m in diameter. The white solar shield of its highest air temperature sensor is seen in the foreground.

DATA AND METHODS. *Craters.* A Davis weather station was installed on the floor of Pu'uwēkiu (19°49.157′N, 155°28.177′W) to record air temperature, humidity, wind speed, and wind direction (Eaton and Businger 2014). Anemometer and temperature sensors were 1 m above ground level. The data are archived online (http://mkwc.ifa.hawaii.edu/archive/wx/wekiu/). Ground temperatures were recorded in Pu'uwēkiu over multiple years (Hobo model U23-003, averaging interval: 30 min).

Meteorological measurements are also available from a weather tower operated jointly by the Canada–France–Hawaii Telescope (CFHT) and the Gemini Observatory. It is located near the summit (Fig. 1) and henceforth will be referred to as the "CFHT tower" (http://mkwc.ifa.hawaii.edu/archive/wx/cfht/). The Vaisala HMP45A humidity and temperature sensor is 3 m above ground level, and the Hydro-Tech anemometer is mounted atop the tower. Two years of data were cleaned up and averaged at half-hour
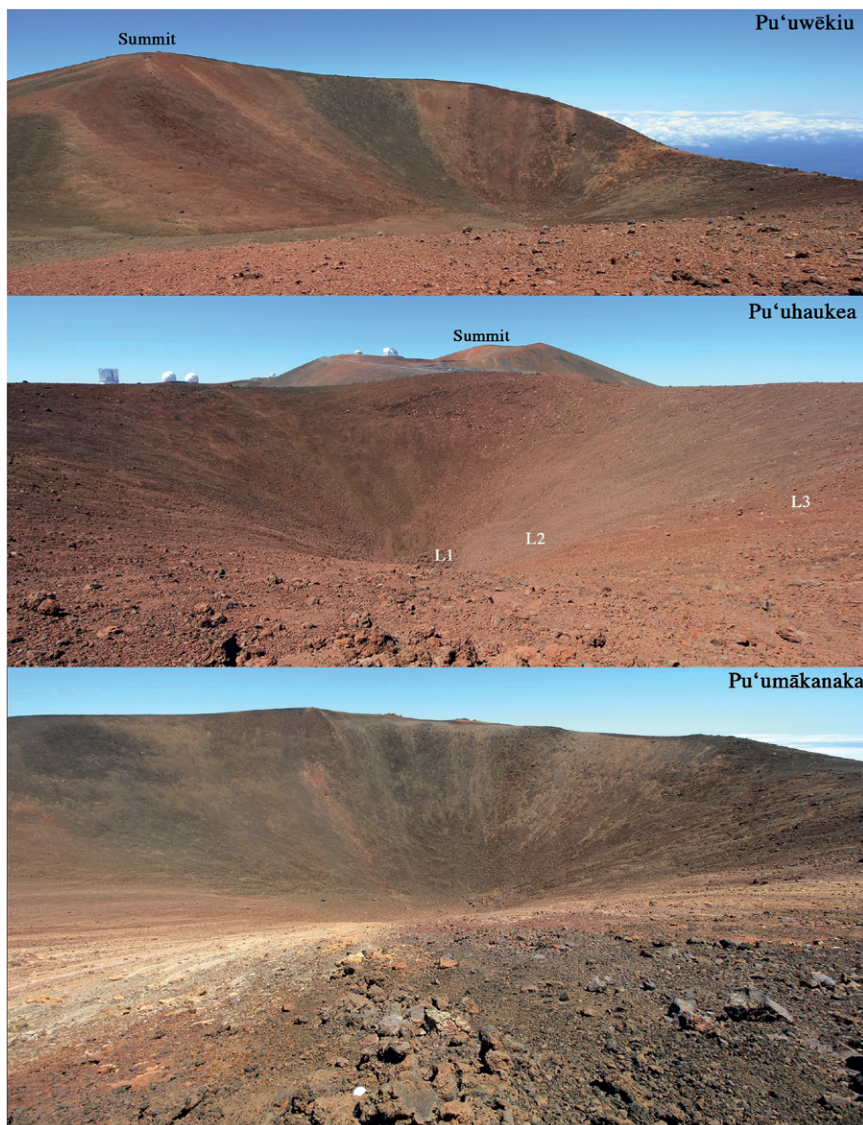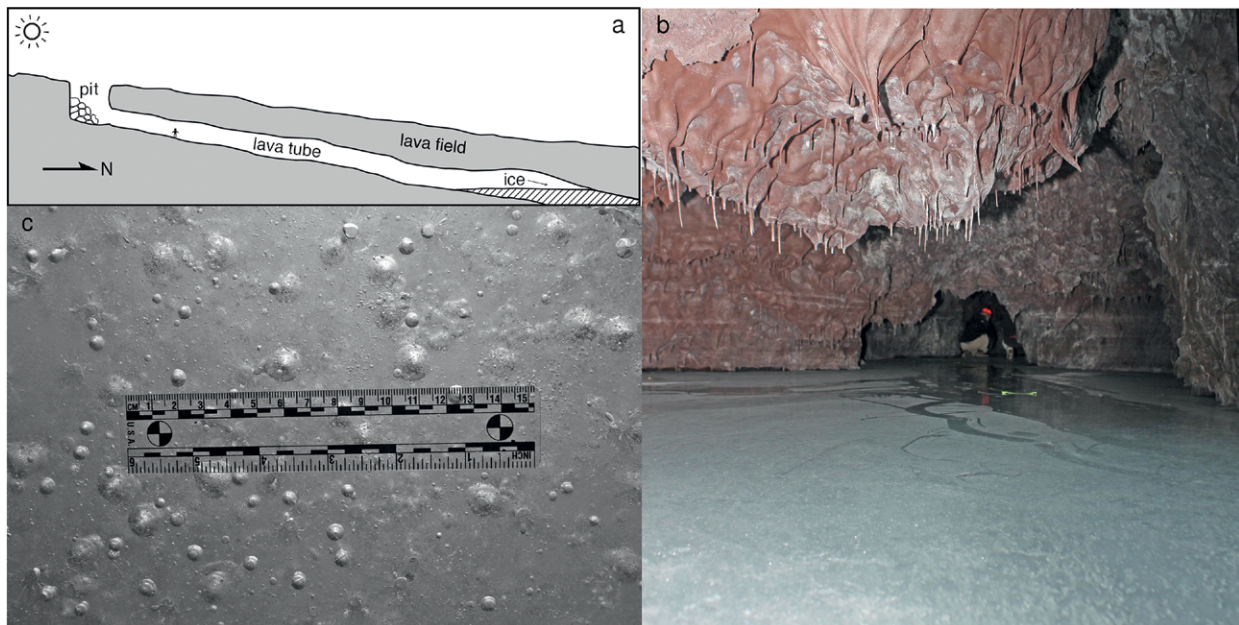
Fɪɢ. 3. (a) Schematic illustration of the geometry of the two branches of Arsia Cave, (b) photo of the ice pond in branch B of Arsia Cave, with a person in the background (22 Apr 2012), and (c) centimeter-sized air bubbles in the same ice pond (23 Nov 2013).

intervals for comparison with the Davis station data, and to calculate the abovementioned freezing index.

From 2013 to 2016, air temperature sensors with solar radiation shields (Onset RS3-B) were operated near ground level at three elevations inside Puʻuhaukea Crater (Hobo models U23-002 and U23-003): on the crater floor, on the north-facing interior slope (about 8 m above the floor), and near the crater rim (about 24 m above the floor) (Figs. 1 and 2). These same sensors were emplaced in Puʻumākanaka from May to November 2016. The elevation differences were 20 m between the floor and the middle sensor and 63 m between floor and the rim logger. Data were archived by Schörghofer and Yoshikawa (2017).

All reported times are local standard times. Wind speeds are recorded in whole values of miles per hour (mph), so the lowest nonzero value is 0.4 m s^{-1} (1 mph). Nighttime and daytime measurements are separated based on sunrise and sunset times calculated with the algorithm by Blanco-Muriel et al. (2001), where night is defined as between sunset and sunrise on a flat horizon. Interferometric synthetic aperture radar (InSAR) data from Intermap Technologies provided topography at a resolution of 4.5 m × 4.5 m. Sky view factors are calculated from these topographic data based on horizon heights along 180 azimuth rays. Drainage basin areas are determined computationally by following the direction of the steepest descent based on the eight neighboring cells.

Caves. Results for the ice caves are based on biannual field visits from November 2011 to April 2015. Three lava tube branches with ice ponds were instrumented with dataloggers with external temperature and relative humidity sensors (Table 2); the data are archived at Schörghofer (2017). All three entrance pits were instrumented with two-channel temperature dataloggers, with one sensor close to the floor and the other placed at the maximum reachable height. Air temperatures were also recorded immediately above each of the three ice bodies. During several visits the ice surface temperature was measured with a ribbon

TABLE 2. List of air temperature *T* and relative humidity (RH) sensors for the cave microclimate study.

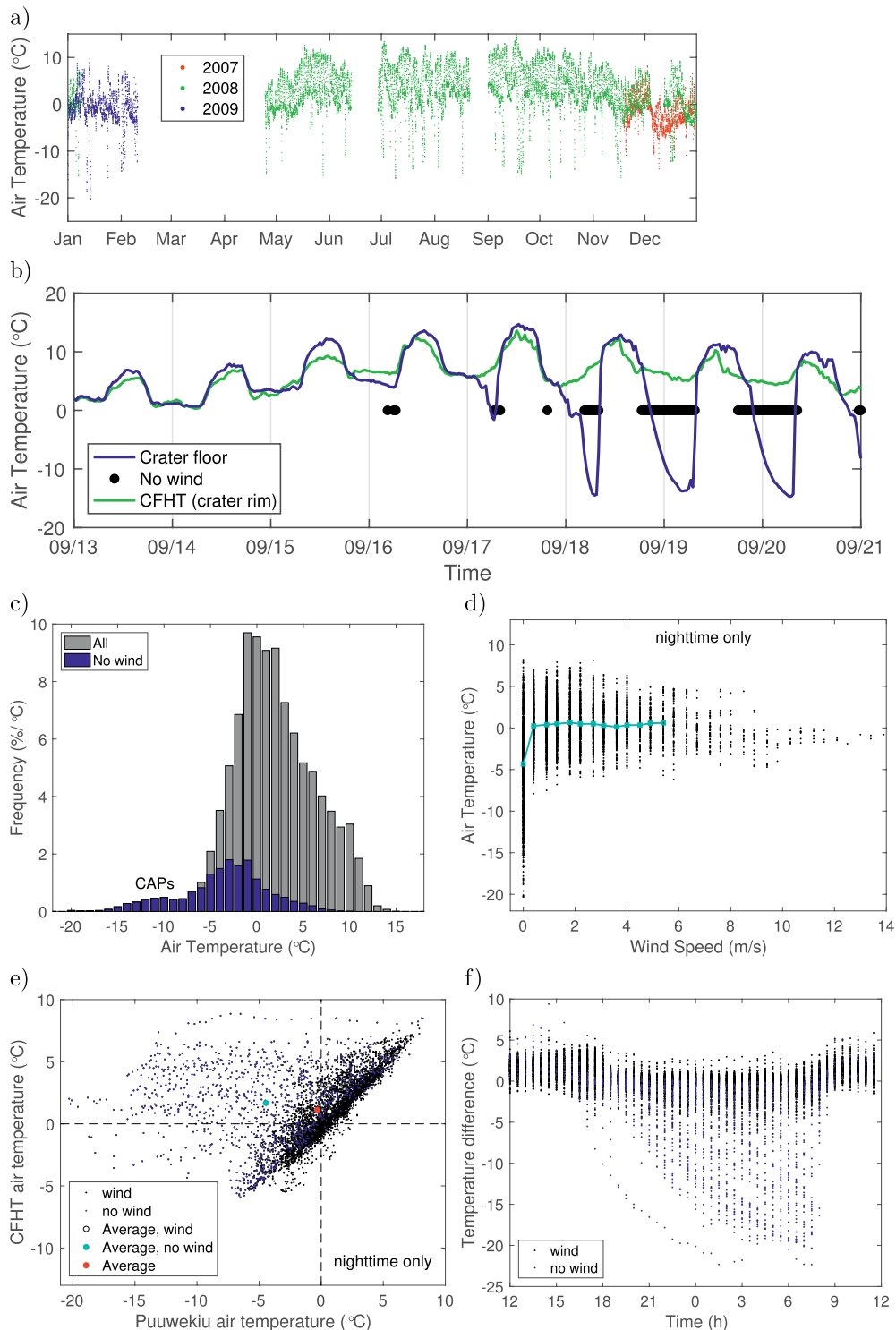| Lava tube	Location	Sensors (averaging interval)	Height difference (m)	Hobo logger model
Mauna Loa Icecave	Entrance	*T* × 2 (30 min)	2.5	UI2-008
	Ice body	RH, *T* (30 min)	—	U23-002
Arsia Cave, branch A	Entrance	*T* × 2 (30 min)	3.2	UI2-008
	Ice body	RH, *T* (10, 30 min)	—	H21-002, U23-002
Arsia Cave, branch B	Entrance	*T* × 2 (30 min)	3.6	UI2-008
	Ice body	RH, *T* (30 min)	—	U23-002

Fig. 4. Microclimate analysis of Pu'uwēkiu Crater. (a) Available time series of air temperature at the crater floor. (b) Air temperature over eight consecutive days in Sep 2008. Black dots indicate periods when wind was <0.4 m s⁻¹ on the crater floor. (c) Histogram of all air temperatures measured on the crater floor (gray). Measurements without detectable wind are shown in blue. (d) Half-hour-mean air temperature as a function of wind speed on the crater floor (black dots) and the means for each bin (blue line). The wind speeds are discretized in units of mph (1 mph ≈ 0.45 m s⁻¹). Means were calculated only if at least 96 measurements (48 h) were available. (e) Relation between half-hour-mean temperatures measured at the CFHT tower located outside the crater and at the Pu'uwēkiu station on the floor of the crater. (f) The difference between the CFHT and Pu'uwēkiu station data as a function of time.

surface probe from ThermoWorks, THS-103-030. The same probe immersed in liquid water above ice in the cave reported a temperature of +0.1°C. MLO provides excellent data to characterize the overall climate of this environment. Hourly station temperatures at 2 m above ground level are used (ftp://aftp.cmdl.noaa.gov/data/meteorology/in-situ/mlo/).

COLD-AIR POOLS IN CINDER CONE CRATERS. *Puʻuwēkiu: Temperature–wind relation.*

Weather station data from the floor of Puʻuwēkiu are available from November 2007 to February 2009, with some gaps (Fig. 4a). The minimum recorded temperature was –20.3°C, on 14 January 2009, the lowest temperature ever reported from the Hawaiian Islands. On windless nights, air temperatures on the crater floor fall considerably. For example, on the night of 17/18 September 2008 (Fig. 4b), no cold-air pool had formed by midnight, but as soon as the wind dropped in the early morning hours, the temperature fell rapidly. The next night, calm conditions set in earlier and cold pool formation started at sunset. No such temperature drops occurred outside the crater, as indicated by the CFHT tower data. At nights when a cold pool forms, cooling typically proceeds at 1°C h^{-1}.

The histogram of air temperatures (Fig. 4c) shows a bimodal distribution with a pronounced tail at low temperatures. Exceptionally cold temperatures require stagnant air; temperatures below –8°C occur only when there is no detectible wind, and only higher temperatures occur with wind. Temperature was below –8°C for 3% of the total time or 5% of the nighttime. Figure 4d shows the data points and means for each velocity bin, which reveals that calm nights are on average 5°C colder. With increased anemometer sensitivity, this difference may be even larger.

The meteorological data from the CFHT tower (Fig. 1) can be compared with wind and air temperature data from the station on the crater floor. Because the CFHT tower and the Puʻuwēkiu station have considerable data gaps, only simultaneous data are used. Periods having greater than 80% humidity at the crater floor are omitted, because they may correspond to rain, snowfall, or snow cover on the crater floor. Wind speeds at CFHT and the Puʻuwēkiu station are strongly correlated (correlation coefficient $r = 0.81$) and, as expected, higher at the crater rim than at the crater floor, by a factor of 3.9 at night (not shown). Air temperatures are also strongly correlated ($r = 0.86$ for >0.4 m s^{-1}), except when winds are calm ($r = 0.15$ for <0.4 m s^{-1}) (Fig. 4e). The difference between the two temperatures as a function of time (Fig. 4f) brings out the disparity during calm nights. The temperature can be considerably lower at the crater floor (Puʻuwēkiu station) than at the crater rim (CFHT tower), and by extrapolation the nearby summit of Mauna Kea.

Puʻuhaukea and Puʻumākanaka: Depth dependence. Air temperature sensors were installed at several heights in Puʻuhaukea and Puʻumākanaka, but no wind data were collected within these craters. In both craters, the air temperature exhibits the same characteristic behavior as in Fig. 4b. On most nights all sensors have approximately the same temperature, but on some nights the crater floor gets exceptionally cold, and the minimum temperatures at the crater floor are significantly below those on the outside. Table 3 lists measured temperature minima. On the floor of Puʻuhaukea, air temperature was below –8°C again about 3% of the time (October 2013–January 2016), and the lowest temperature measured was –18°C. The Puʻumākanaka measurement period did not include the winter months, so the minimum temperature over a year is likely lower.

The uppermost sensor at Puʻumākanaka was situated higher than the lowest point on the crater rim, something that was not the case at Puʻuhaukea (Fig. 1), so it can be expected to always be above the CAP. Hence the temperature difference between this sensor and that at the crater floor serves as a measure of the strength of the cold-air pool. At

TABLE 3. Air temperatures at Hawaii's coldest places and nearby locations. The CFHT weather tower, the rim of Puʻumākanaka, and MLO are included for comparison. An asterisk indicates that calculations are affected by significant data gaps.

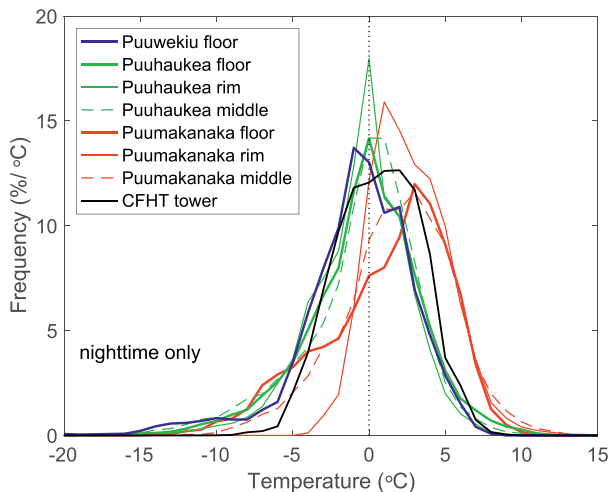| Site	Period	Min (°C)	Mean (°C)	Time below freezing (%)
CFHT tower	1 Jan 2007–31 Dec 2008	–11	+2.1	29
Puʻuwēkiu (floor)	20 Nov 2007–9 Feb 2009*	–20	—	36
Puʻuhaukea (floor)	7 Oct 2013–29 Jan 2016	–18	—	33
Puʻumākanaka (floor)	5 May–2 Nov 2016	–14	—	20
Puʻumākanaka (rim)	5 May–2 Nov 2016	–4	—	8
MLO	1 Jan 2011–31 Dec 2015	–5	+7.7	1
Mauna Loa Icecave	1 Jan 2012–31 Dec 2014*	–1.1	+0.1	43
Arsia Cave (branch A)	1 Jan–31 Dec 2012	–1.1	–0.7	100

Fɪɢ. 5. Histograms of all nighttime air temperature measurements considered in the crater microclimate study. The area under each histogram is unity.

Puʻumākanaka the extreme minimum temperature is 10°C higher at the rim than at the crater floor.

Figure 5 shows the nighttime temperature histograms of all air temperature time series. The histogram for Puʻuwēkiu (blue) can be compared with that of the CFHT tower (black). Puʻuhaukea has a temperature distribution (green) similar to that of Puʻuwēkiu. For Puʻumākanaka (red), there is an excess of cold temperatures at the floor compared to its crater rim. In the deepest crater, CAPs are no stronger, but the histograms suggest they are more frequent than in the other two craters.

Discussion. The Puʻuwēkiu station data suggest that CAPs <−8°C occur 3% of the time and cause, on average, 5°C of cooling. These numbers are not corrected for the uneven distribution of data records over the year, but CAPs occur during every season. The estimated contribution to the MAAT is the product of these two numbers, about −0.1°C. The difference between crater floor temperatures with and without the temperature $T < -8$°C tail is 0.4°C on average. By either estimate, CAPs are only minor contributors to the annual-mean temperature.

A CAP can be maintained when the wind shear does not exceed the stratification strength. The stratification is characterized by the Brunt–Väisälä frequency N, defined as $N^2 = (g/\Theta)(d\Theta/dz)$, where g is the gravitational acceleration constant, Θ is potential temperature, and z is vertical distance. A criterion for stability is

$$\frac{\overline{u}}{h} \leq F_c N, \qquad (1)$$

where h is the height of the valley walls, $\overline{u}$ is the horizontal velocity, and $F_c = 1.3$ is the critical Froude number (Bell and Thompson 1980). The CAPs in deeper basins can withstand higher wind speeds and are hence expected to be more frequent. As the strength of the CAP increases during the night, the theoretical wind speed threshold increases with time.

In environments with little snow, a surface layer of coarse boulders lacking fines is often associated with permafrost (Harris and Pedersen 1998). Figure 6a shows a vertical transect through the surface layer. Boulder sizes are typically in decimeters. Voids between coarse blocky materials allow air to move through more easily, which can cause cooling as a result of settling of dense cold air. Ventilation can also enhance evaporation or sublimation, creating a heat sink.

Figure 6b shows temperatures from a two-channel datalogger at the bottom of the permafrost slope in Puʻuwēkiu. The upper sensor is exposed at a shallow depth among the boulders, and the lower sensor is buried in finer material 40 cm below the surface and does not reach into the permafrost. The figure also includes air temperatures from the CFHT tower near the crater rim. The comparison of the three temperatures reveals that the air temperature among boulders falls to considerably lower temperatures than the air outside the crater, especially on nights without wind. This suggests that cold air accumulates in the interstitial spaces. The temperature of the lower sensor is damped and delayed compared to the shallower sensor but has an average lower than the other two temperatures. The 2014 annual means were +3.3°C (crater rim), +2.5°C (shallow sensor), and −0.2°C (deeper sensor). This suggests a net cooling takes place between the upper and lower sensors. A similar behavior to Fig. 6b is also found 5 m upslope, where another datalogger was emplaced. Because of the relation with calm conditions, the cooling effect of the coarse blocky material must be due to cold air settling.

THE ICE CAVES OF MAUNA LOA VOLCANO. The ice ponds in Arsia Cave completely block the lava tubes (Fig. 3). During daytime visits the air temperature drops monotonically from the entrance toward the ice chamber. The environment in the deep parts of the caves is nearly isothermal. The surface temperature of the ice ponds ranged from −0.7° to 0°C, the same as the air temperature. In contrast to Arsia Cave, MLIC has an intermittent airflow related to fluctuating ice levels, as described by Pflitsch et al. (2016). The surface of the ice plug in MLIC melts routinely, but the ice beneath is perennial.
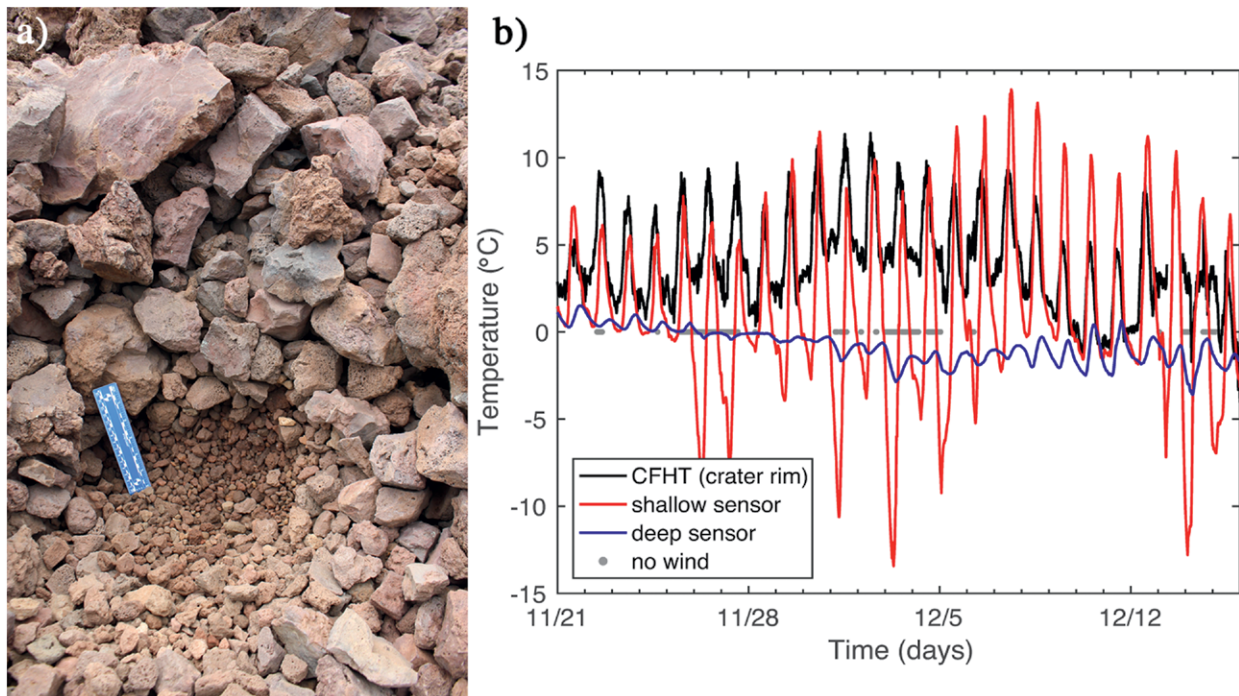
Fig. 6. (a) Coarse blocky material above the permafrost in Puʻuwēkiu. The pit exposes a ~30-cm-thick coarse layer with finer material beneath. A 15-cm (6 in.) ruler is included for scale. (b) Air temperature on the crater rim (1-min intervals) compared with the air temperature among the boulders at shallow depth and temperatures at 40-cm depth in the finer material (half-hour intervals) for 25 days in Nov and Dec 2015 (Logger wek774). Periods with winds <0.4 m s⁻¹ at the CFHT tower are indicated by gray dots.

At −0.7°C, Arsia Cave holds the record for the lowest annual-mean temperature ever reported for Hawaii (Table 3). The temperatures above the ice pond in part B of Arsia Cave are slightly above those in part A (Fig. 7), but these measurements also started later, and the air in both ice chambers gradually warmed over the years. In 2012 the annual-mean humidity in ice chamber A was 90%, and its humidity varied between 60% and 100%.

To explore the cooling mechanism of the ice caves, the air temperature at the entrances is compared with that at MLO and above the ice bodies in Fig. 7. These temperature time series immediately lead to two conclusions. First, the entrance pit floors are significantly colder than the outside environments (cf. MLO temperature with entrance temperature). The annual averages for 2012 are as follows: MLO: +7.6°C, floor of Arsia Cave branch A entrance: +4.6°C, and floor of MLIC entrance: +4.5°C. Hence, the entrance pits account for 3°C of cooling. Second, the temperature at the entrance rarely falls below freezing, which suggests that the cold air sinking into the lava tubes cannot reach the ice chambers. The air column in the deep parts of the lava tubes is expected to be stagnant throughout most of the year.

Microclimate of the entrance pits. To better understand the role of the entrance pits, a single week of data is shown in Fig. 8b. The entrance floor temperatures follow drops in the outside temperature during the night, but they do not rise to high temperatures during the day. Hence, the air in the entrance pit is stratified during the day and not mixed by wind shear.

The entrance pit is shadowed and the warmest air never reaches the floor of the pit or the cave entrance (Fig. 8). In light of Eq. (1), it is surprising that cold air frequently persists in the pits; the entrance pits are only on the order of 10 m deep and therefore should be ventilated even more frequently than the deeper craters on Mauna Kea. The cold air does not pool over the entire depth of the pit but only near the floor. Further evidence for this is found in the temperature difference between the two sensors at the entrance. At all three entrance pits, the higher sensor is generally warmer than the sensor at the floor by 1°C. The collapsed ceilings of the entrance pits fill them with blocky material that may store cold air in the interstitial spaces (Fig. 8a).

Winter night's cold theory. Here we narrow our investigation to the two branches of Arsia Cave, because the MLIC is more dynamic in character. Because of the

small seasonal temperature amplitude in the tropics (Fig. 7), the winter's cold theory may be more appropriately called the "night's cold theory," or, better, the "winter night's cold theory." While this theory appears applicable for past years, pit temperatures now rarely fall below freezing, so this is not a plausible explanation for the perennial cave ice in the present climate.

MLO temperatures were lower a few decades ago. During the period 1977–2006 there was a near-uniform warming of 0.040°C yr^{-1} for nighttime data (Malamud et al. 2011). Extrapolating this trend to 2015, it amounts to a 1.5°C increase in nighttime temperatures since 1977, whereas the trend before the 1970s was much slower. Subfreezing night temperatures must have been significantly more common, and might have even occurred in summer.

Moist air is less dense than dry air at the same temperature, because the molecular weight of H$_2$O is 18 g mol^{-1} compared to 29 g mol^{-1} for dry air. At the elevation of MLO the total pressure is 680 hPa, and the saturation vapor pressure at freezing is 6.1 hPa. The relative density difference between dry and fully saturated air at 0°C is $\Delta\rho/\rho = 6.1 \times (18 - 29)/(680 \times 29)$. Also, according to

the ideal gas law, a small temperature difference ΔT causes a relative density difference of $\Delta\rho/\rho = -\Delta T/T$. Hence, at this elevation, a fully saturated air parcel has a density equivalent to that of a dry air parcel $\Delta T \approx 1°C$ warmer. Dry air colder than +1°C may sink all the way down the lava tube to an ice chamber with saturated air at 0°C. This is a maximum number, as the actual humidity difference between the inside and outside air is always less than 100%, but nevertheless the contribution of vapor buoyancy is nonnegligible. The addition of dry air, even if above freezing
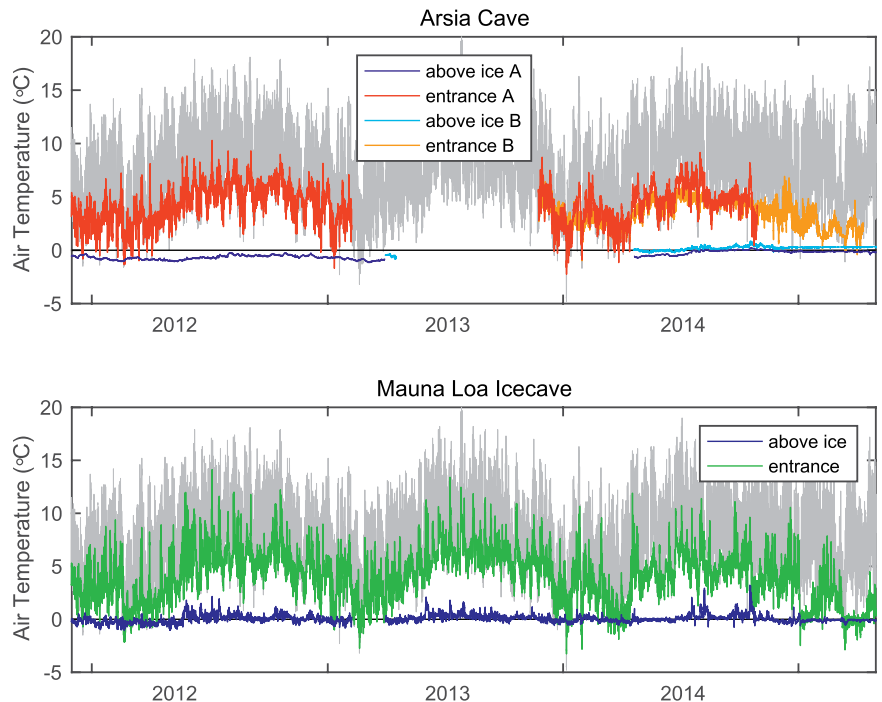

FIG. 7. Air temperature time series at the floor of three lava tube entrances (red, orange, and green) and at the three corresponding ice bodies (blue, light blue, and dark blue) from 1 Dec 2011 to 30 Apr 2015. The gray graph in the background is MLO air temperature.
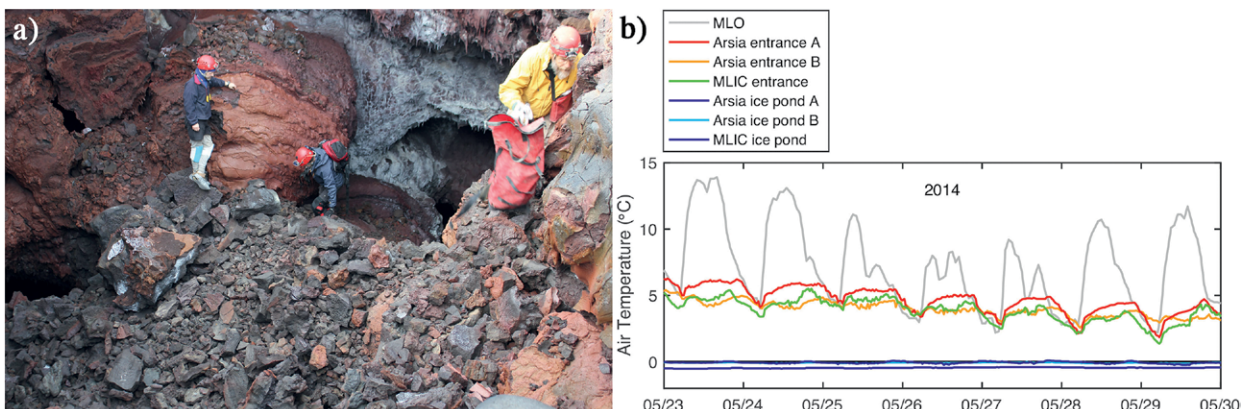

FIG. 8. (a) Breakdown material at the entrance pit of Arsia Cave branch B. (b) Air temperature time series over one week, illustrating how temperature at the floor of the pit responds to the outside temperature.

temperature, would help remove vapor from the ice chamber and enhance evaporative cooling. In this case, the ratio of sensible to latent heat, also known as the Bowen ratio, is negative (Andreas and Cash 1996).

When the air in the entrance pit is colder than the air in the lava tube, a gravity current of negatively buoyant cold air will flow down the tube that typically fills only half the height of the tube (Simpson 1982). With a molecular diffusivity of $D \sim 0.2 \times 10^{-4} \times 1{,}013/680 \sim 0.3 \times 10^{-4}\,\mathrm{m^2\,s^{-1}}$ (Massman 1998), air will mix during half a day t over a distance of $\sqrt{2Dt} \sim 1.6$ m, and molecular diffusivity is only a lower limit on the actual diffusivity. Even without entrainment and turbulent mixing, any gravity current would mix diffusively throughout the diameter of the tube. Hence, the air deep in the cave can be expected to be well mixed vertically, precluding simultaneous movement of cold air in the lower part of the tube and warm air in the upper half of the tube in the opposite direction.

Microclimate of the ice chambers. Water occasionally drips on the ice pond and then freezes and sublimates or it may freeze, thaw, and evaporate. Either way, it enters in liquid form and leaves in vapor form, and the enormous difference in latent heat cools the ice pond. As far as we could discern from visual inspection, there is no outlet/loss of water in liquid form. Water vapor could escape through the lava tube, but the air at the entrance pit is almost always lighter than the air in the ice chamber. Water vapor could escape through pathways in the ceiling, possibly using the same pathways by which liquid water reaches the ice chamber. Or the vapor could recondense on the ceiling where the heat is shed upward, so the ice pond would still experience a net cooling. If little vapor escapes the cave, then the chamber must gradually fill with water or ice. The present-day precipitation rate at MLO is 0.45 m yr⁻¹ (http://rainfall.geography.hawaii.edu), and only a tiny fraction of that will enter the cave. Hence, it is plausible that the ice ponds have gradually grown over centuries.

Since subfreezing temperature is rarely available on the surface in the current climate, evaporation of vapor must be the dominant form of cooling. When the humidity rises to 100%, evaporative cooling ceases, so the ice chambers need to be sufficiently ventilated with unsaturated air for the ice to remain frozen. The temperature difference over the height of the entrance pits plays no role, because it affects only daytime temperatures. The evaporative cooling effect will also apply to water ponds rather than ice ponds, although we do not know of any such cave on Mauna Loa.

The air temperatures above both ice bodies in Arsia Cave reached the melting point in summer 2014 (Fig. 7). Indeed, during the following visit in November 2014 we observed meltwater on ice pond A and white ice (indicating recent freezing) for the first time. Ice pond B had so much meltwater we could not cross it.

The rising temperatures (both mean and nighttime), the lack of subfreezing outside air temperatures, the measured warming of the air above the ice ponds, and the observed recent melting coherently point toward evaporative cooling being insufficient to keep the ponds in a frozen state. The two ice bodies of Arsia Cave are expected to fall victim to climate warming, unless receding ice levels will open up passages on the other end of the ice chambers, which would lead to more airflow and enhance evaporative cooling. The MLIC is a cave in this microclimate state.

CONCLUSIONS. The lowest temperatures in the Hawaiian Islands occur within a cinder cone crater near the summit of Mauna Kea. Nocturnal cold-air pools create extreme temperature minima on calm nights. The strength of the pool increases throughout the night, until the cold-air pool is destroyed at sunrise. Although nocturnal cold-air pools are not uncommon and occur during all seasons, they are too infrequent to significantly lower the annual-mean temperature. The more frequent trapping of cold nighttime air in interboulder spaces above the permafrost has a more significant impact on the annual-mean temperature. The trapping of air in interboulder spaces also depends on wind speed, but it can sustain higher wind speed thresholds. Shelter from strong winds within a crater can cause a preference, among north-facing slopes with terrain shadowing, for permafrost inside crater basins.

Perennial ice is found in caves on Mauna Loa at even lower altitudes than the permafrost on Mauna Kea. The lowest annual-mean temperature ever measured in the Hawaiian Islands is at the terminal end of branch A of Arsia Cave. In the climate that prevailed up to a few decades ago, nighttime temperatures were low enough for cold dry air to sink all the way to the humid ice chambers, frequently in winter and perhaps occasionally even in summer. In the current climate, this is no longer the case, and cooling must currently primarily be due to the evaporation of the ice. After being frozen for many years, the ice bodies in Arsia Cave have begun to melt, which suggests that evaporative cooling alone may be insufficient to maintain freezing conditions in the long term. The buoyancy of water vapor plays a role in the microclimate in Arsia Cave, because it helps to ventilate the ice chamber
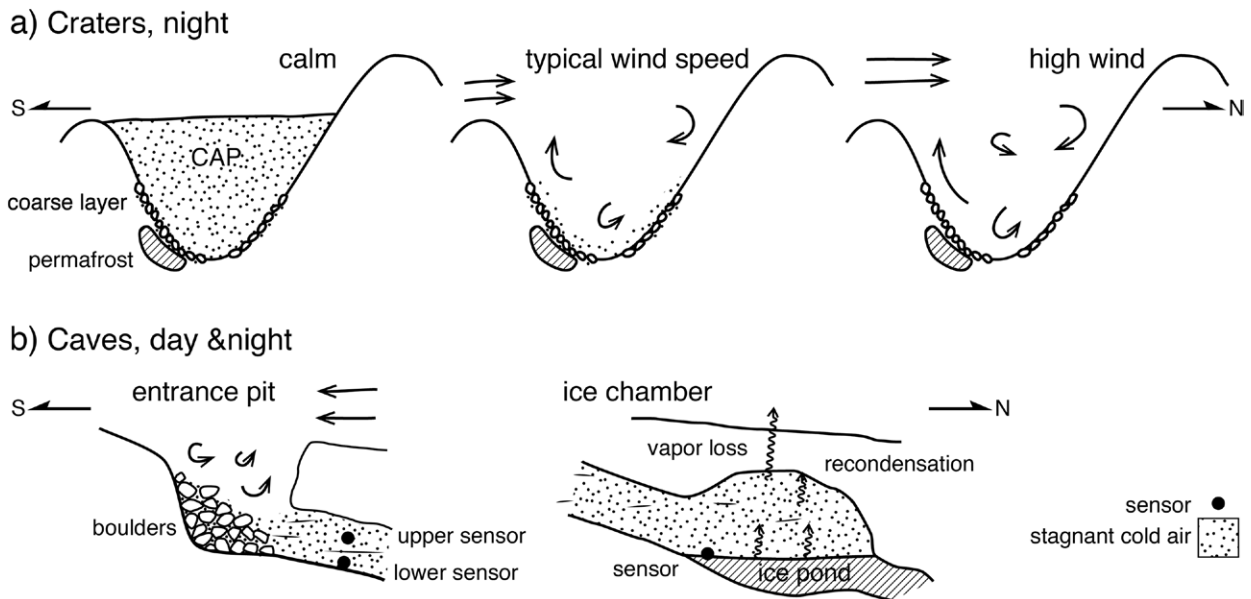
FIG. 9. Schematic illustrations of inferred ventilation and cold-air accumulation in high-altitude ice-preserving microclimates on the island of Hawaii. (a) Craters (vertically exaggerated) can accumulate radiatively cooled air at night. This exceptionally cold air resides in the porous subsurface even at moderate wind speed. (b) The lava tube entrance pits, smaller than the craters, are ventilated, but cold air remains near the floor all day. In the current climate, the ice ponds remain frozen almost exclusively because of evaporative cooling. The short horizontal lines indicate stratification. The ice chamber microclimate illustrated here is representative of the two branches of Arsia Cave.

and therefore enhances evaporative cooling. Even though the dry air may be warmer than the humid air it replaces, the net effect can be heat removal. The airflow delivers sensible heat to the ice but carries away the latent heat stored in the vapor.

Accumulation of cold air is a pervasive phenomenon for the coldest known microclimates on the tall volcanoes of Hawaii (Fig. 9). Basinwide cold-air pooling plays no significant role in the preservation of the perennial ice, neither in the craters nor in the cave entrance pits, but negatively buoyant air near and below the surface does. One wonders whether the diurnal, rather than seasonal, character of these cold-air flows makes heat removal particularly efficient.

REFERENCES

Andreas, E. L, and B. A. Cash, 1996: A new formulation for the Bowen ratio over saturated surfaces. *J. Appl. Meteor.*, **35**, 1279–1289, https://doi.org/10.1175/1520 -0450(1996)035<1279:ANFFTB>2.0.CO;2.

Balch, E. S., 1900: *Glacières or Freezing Caverns.* Allen, Lain & Scott, 337 pp.

Bari, S. A., and J. Hallett, 1974: Nucleation and growth of bubbles at an ice-water interface. *J. Glaciol.*, **13**, 489– 519, https://doi.org/10.1017/S0022143000023248.

Bell, R. C., and R. O. Thompson, 1980: Valley ventilation by cross winds. *J. Fluid Mech.*, **96**, 757–767, https:// doi.org/10.1017/S0022112080002340.

Blanco-Muriel, M., D. C. Alarcón-Padilla, T. López-Moratalla, and M. Lara-Coira, 2001: Computing the solar vector. *Sol. Energy*, **70**, 431–441, https://doi .org/10.1016/S0038-092X(00)00156-0.

Carte, A. E., 1961: Air bubbles in ice. *Proc. Phys. Soc.*, **77**, 757–768, https://doi.org/10.1088/0370-1328/77/3/327.

Clements, C. B., C. D. Whiteman, and J. D. Horel, 2003: Cold-air-pool structure and evolution in a mountain basin: Peter Sinks, Utah. *J. Appl. Meteor.*, **42**, 752–768, https://doi.org/10.1175/1520-0450(2003)042<0752:CSAEIA>2.0.CO;2.

Eaton, L. A., and S. Businger, 2014: Using a snow drift model to simulate eolian drift and snowfall on the summit of Mauna Kea, Hawaii. *Arct. Antarct. Alp. Res.*, **46**, 719–734, https://doi.org/10.1657/1938-4246-46.4.719.

Geiger, R., R. H. Aron, and P. Todhunter, 2009: *The Climate Near the Ground*. 7th ed. Rowman & Littlefield, 623 pp.

Halliday, W. R., 2004: Hawaii lava tube caves, United States. *Encyclopedia of Caves and Karst Science*, J. Gunn, Ed., Fitzroy Dearborn, 858–862.

Harris, S. A., 1981: Climatic relationships of permafrost zones in areas of low winter snow-cover. *Arctic*, **34**, 64–70, https://doi.org/10.14430/arctic2507.

——, and D. E. Pedersen, 1998: Thermal regimes beneath coarse blocky materials. *Permafrost Periglacial Processes*, **9**, 107–120, https://doi.org/10.1002/(SICI)1099-1530(199804/06)9:2<107::AID-PPP277>3.0.CO;2-G.

Malamud, B. D., D. L. Turcotte, and C. S. B. Grimmond, 2011: Temperature trends at the Mauna Loa observatory, Hawaii. *Climate Past*, **7**, 975–983, https://doi.org/10.5194/cp-7-975-2011.

Massman, W., 1998: A review of the molecular diffusivities of H_2O, CO_2, CH_4, CO, O_3, SO_2, NH_3, N_2O, NO, and NO_2 in air, O2 and N2 near STP. *Atmos. Environ.*, **32**, 1111–1127, https://doi.org/10.1016/S1352-2310(97)00391-9.

Neff, W. D., and C. W. King, 1989: The accumulation and pooling of drainage flows in a large basin. *J. Appl. Meteor.*, **28**, 518–529, https://doi.org/10.1175/1520-0450(1989)028<0518:TAAPOD>2.0.CO;2.

Niu, F., G. Cheng, Y. Niu, M. Zhang, J. Luo, and Z. Lin, 2016: A naturally-occurring 'cold earth' spot in Northern China. *Sci. Rep.*, **6**, 34 184, https://doi.org/10.1038/srep34184.

Persoiu, A., and B. P. Onac, 2011: Ice in caves. *Encyclopedia of Caves*, W. B. White and D. C. Culver, Eds., Academic Press, 399–404.

Pflitsch, A., N. Schörghofer, S. M. Smith, and D. Holmgren, 2016: Massive ice loss from the Mauna Loa Icecave, Hawaii. *Arct. Antarct. Alp. Res.*, **48**, 33–43, https://doi.org/10.1657/AAAR0014-095.

Sauberer, F., and I. Dirmhirn, 1954: Über die Entstehung der extremen Temperaturminima in der Doline Gstettner-Alm. *Arch. Meteor. Geophys. Bioklimatol.*, **5B**, 307–326.

Schörghofer, N., 2017: Multi-year temperature and humidity time series from ice caves on Mauna Loa, Hawaii. Zenodo, https://doi.org/10.5281/zenodo.833546.

——, and K. Yoshikawa, 2017: Multi-year temperature time series from five cinder cones on the Mauna Kea summit plateau, Hawaii. Zenodo, https://doi.org/10.5281/zenodo.883470.

——, M. Leopold, and K. Yoshikawa, 2017: State of permafrost on tropical Maunakea volcano, Hawaii. *Permafrost Periglacial Processes*, **28**, 685–697, https://doi.org/10.1002/ppp.1954.

Simpson, J. E., 1982: Gravity currents in the laboratory, atmosphere, and ocean. *Annu. Rev. Fluid Mech.*, **14**, 213–234, https://doi.org/10.1146/annurev.fl.14.010182.001241.

Teehera, K. B., and Coauthors, 2018: Cryogenic minerals in Hawaiian lava tubes: A geochemical and microbiological exploration. *Geomicrobiol. J.*, **35**, 227–241, https://doi.org/10.1080/01490451.2017.1362079.

Whiteman, C. D., T. Haiden, B. Pospichal, S. Eisenbach, and R. Steinacker, 2004: Minimum temperatures, diurnal temperature ranges, and temperature inversions in limestone sinkholes of different sizes and shapes. *J. Appl. Meteor.*, **43**, 1224–1236, https://doi.org/10.1175/1520-0450(2004)043<1224:MTDTRA>2.0.CO;2.

——, and Coauthors, 2008: METCRAX 2006: Meteorological experiments in Arizona's Meteor Crater. *Bull. Amer. Meteor. Soc.*, **89**, 1665–1680, https://doi.org/10.1175/2008BAMS2574.1.

——, S. W. Hoch, M. Lehner, and T. Haiden, 2010: Nocturnal cold-air intrusions into a closed basin: Observational evidence and conceptual model. *J. Appl. Meteor. Climatol.*, **49**, 1894–1905, https://doi.org/10.1175/2010JAMC2470.1.

Woodcock, A. H., 1974: Permafrost and climatology of a Hawaii volcano crater. *Arct. Alp. Res.*, **6**, 49–62, https://doi.org/10.2307/1550369.

——, 1987: Mountain breathing revisited—The hyperventilation of a volcano cinder cone. *Bull. Amer. Meteor. Soc.*, **68**, 125–130, https://doi.org/10.1175/1520-0477(1987)068<0125:MBRHOA>2.0.CO;2.

——, and I. Friedman, 1979: Mountain breathing—Preliminary studies of air-land interaction on Mauna Kea, Hawaii. Shorter Contributions to Geophysics, 1979, Geological Survey Professional Paper 1123, U.S. Geological Survey, A1–A8, https://pubs.usgs.gov/pp/1123a-d/report.pdf.

——, A. S. Furumoto, and G. P. Woollard, 1970: Fossil ice in Hawaii? *Nature*, **226**, 873, https://doi.org/10.1038/226873a0.